


# Thermal cycling testing of Zn–Mg–Al eutectic metal alloys as potential high-temperature phase change materials for latent heat storage

E. Risueño<sup>1</sup> · A. Gil<sup>1</sup> · J. Rodríguez-Aseguinolaza<sup>1</sup> · A. Gil<sup>1</sup> · M. Tello<sup>2</sup> · A. Faik<sup>1</sup>  · B. D'Aguanno<sup>1</sup>

Received: 6 June 2016 / Accepted: 6 March 2017 / Published online: 14 March 2017  
© Akadémiai Kiadó, Budapest, Hungary 2017

**Abstract** This article presents the thermal stability testing results of five high-temperature phase change materials for their potential use in latent thermal energy storage systems. The tested materials are eutectic metal alloys [ $\text{Zn}_{84}\text{Al}_{8.7}\text{Mg}_{7.3}$ ,  $\text{Zn}_{88.7}\text{Al}_{11.3}$ ,  $\text{Zn}_{92.2}\text{Mg}_{7.8}$ ,  $\text{Zn}_{72}\text{Mg}_{28}$  and  $\text{Mg}_{70}\text{Zn}_{24.9}\text{Al}_{5.1}$  (at.%) with phase change temperatures in the range of 340–380 °C. The five candidates have been selected not only for their adequate melting temperature and high fusion enthalpy, but also for the availability and appropriate costs [2–3 \$/kg (Rodríguez-Aseguinolaza in J Therm Anal Calorim 117:93–99, 2014)] of Zn, Al, and Mg primary metals. As it is well known and demonstrated in previous works, the use of metal alloys presents noticeable benefits on the TES solutions based on their implementation. The particular advantages introduced by the Zn–Mg–Al system in terms of maximization of the storage capacity and appropriate operation temperature justify a deeper analysis of these alloys, previously studied, for a complete thermal performance. In this work, with the aim of reproducing a realistic thermal cycling behaviour in real heat storage applications, the selected candidates have been subjected to short- and long-term thermal cycling tests by 100 and 500 melting/solidification cycles, respectively. These experiments permitted to detect any potential evolution of the thermodynamic and structural properties of the investigated materials that could be sign of an

undesirable chemical decomposition or phase segregation. As a conclusion, the  $\text{Zn}_{84}\text{Al}_{8.7}\text{Mg}_{7.3}$ ,  $\text{Zn}_{88.7}\text{Al}_{11.3}$ ,  $\text{Mg}_{70}\text{Zn}_{28}$  and  $\text{Mg}_{70}\text{Zn}_{24.9}\text{Al}_{5.1}$  alloys have been identified as very promising latent heat storage materials due to their long-term thermal stability.

**Keywords** Thermal stability · Thermal cycling testing · Eutectic metallic alloys · Phase change material · Long-term thermal stability

## Introduction

Latent heat storage (LHS) using phase change material (PCM) has attracted considerable attention during the last four decades, and many types of low-temperature PCMs, mainly with melting temperature below 100 °C, have been extensively studied [2, 3]. However, the potentiality of latent heat thermal storage is not reduced to applications of low operation temperature ranges. The incorporation of thermal energy storage (TES) can improve significantly the thermal efficiency of concentrating solar power (CSP) plants and numerous industrial processes. As consequence, during the last decade the interest in high-temperature LHS has experimented an increase. Michels et al. [4] report experimental and numerical results from the investigation of cascade LHS using nitrate, chloride and hydroxide salts with melting temperature in the range of 306–380 °C for solar power plant application. Seeniraj et al. [5] describe theoretically and numerically charging and discharging characteristics of different types of PCMs with melting temperature in the range of 120–1000 °C for Compact Linear Fresnel Reflector (CLFR) application and Multi-Tower Solar Array (MTSA) technologies. Nomura et al. [6] investigate the feasibility to recover waste heat at

✉ A. Faik  
afaik@cicenergigune.com

<sup>1</sup> CIC Energigune, Albert Einstein 48, 01510 Miñano, Álava, Spain

<sup>2</sup> Dpto. Física de la Materia Condensada, Facultad de Ciencia y Tecnología, Universidad del País Vasco, Apdo. 644, 48080 Bilbao, Spain

temperature over 300 °C in steelworks by sodium hydroxide (NaOH) and to supply it to a benzene, toluene and xylene (BTX) production plant. Kenisarin [7] summarizes the investigation and developments of PCMs with melting temperature from 120 to 1000 °C. Liu et al. [8] review PCMs with melting temperature in the range of 300–550 °C for their potential implementation in the current and under construction CSP plants. Liu et al. [9] combine sensible and latent storage by using concrete composite (maximum operational temperature of 400 °C) and sodium nitrate (NaNO<sub>3</sub>) (melting temperature of 306 °C) for TES in direct steam generation (DSG) plants.

Currently, the under study high-temperature PCMs are inorganic salts, eutectic and non-eutectic inorganic salt mixtures, metals and eutectic and non-eutectic metallic alloys. The salts as high-temperature PCMs have been more extensively investigated than metals, where chlorides, hydroxides and nitrates have reached the greatest interest [7]. However, metal alloys have not been seriously considered as PCMs due to their higher costs compared to the ones of the inorganic salts. Nevertheless, the high volumetric energy density of metal alloys can play an important role when the volume is an important criterion in the thermal storage unit design. Some works [7, 10, 11] consider that the use of metal alloys as PCMs has been underestimated by researchers, although their properties, such as high thermal conductivity, low corrosivity, small volume change and no subcooling, overcome the drawbacks of the salts. Khare et al. [12] use a materials selection software to identify potential PCMs for high-temperature solar energy application (>420 °C). They found that metals such as Al, Mg, Si and Zn and their eutectics are more suitable PCMs than traditional molten salts. The results of this analysis demonstrate that KOH and Zn are the most cost-effective materials. Liu et al. [8] and Hoshi et al. [13] investigate the suitability of high-temperature PCMs for their use in large-scale solar thermal electricity plants. Among their conclusions, it is indicated that Zn may be a cost-effective option for parabolic trough systems using higher boiler temperatures.

To identify potential PCMs, it is essential to study their thermophysical properties, such as phase change temperature, phase-transition latent heat, thermal conductivity or specific heat among others. However, the selection of PCMs must be also performed on basis of their long-term thermal stability. A PCM should be not only thermally, chemically and physically stable, but also should be congruent, which means that no phase segregation or chemical degradation should be happen. In addition, the phase change temperatures should not present great changes and the phase-transition heats should be constant without presenting any decreases in their values. To evaluate the long-term performance of the storage unit, the changes in the

thermophysical properties should be analysed after a repeated number of thermal cycles. In this frame, repeated thermal cycles process performed under controlled conditions in the laboratory is aimed to understand the behaviour of the material under real conditions [14].

Although there are numerous studies of thermal stability for low-temperature PCMs [14–26], investigations for high-temperature PCMs are scarce. Shin et al. [27] analyse the long-term performance of a carbonate eutectic salt with melting temperatures in the range of 395–400 °C up to 50 melting/solidification thermal cycles. Sun et al. [28] determine the thermal stability of Al–34%Mg–6%Zn alloy with melting temperature of 454 °C for 1000 thermal cycles. Kuravi et al. [29] summarize the evaluated PCMs in terms of cycle life and stability. Alam et al. [30] evaluate the thermal stability of encapsulated nitrate salts with melting temperatures in the range of 122–334 °C up to 2200 cycles. Liu et al. [31] determine the thermal stability of carbonate and chloride salts mixtures with melting temperature in the range of 300–600 °C up to 500 thermal cycles.

In this frame, accelerated thermal cycling tests of five PCM candidates [(A) Zn<sub>84</sub>Al<sub>8.7</sub>Mg<sub>7.3</sub>, (B) Zn<sub>88.7</sub>Al<sub>11.3</sub>, (D) Zn<sub>92.2</sub>Mg<sub>7.8</sub>, (E) Zn<sub>72</sub>Mg<sub>28</sub> and (F) Mg<sub>70</sub>Zn<sub>24.9</sub>Al<sub>5.1</sub> (at.%)] have been performed. In this work, the changes on their melting temperatures and heat of fusion values have been analysed after large number of melting/solidification thermal cycles. The main objective is to determine the long-term thermal stability of these PCM candidates to demonstrate their potentiality to be used in real application, where long-term life cycle of storage material is required. In this way, melting temperature and heat of fusion are key properties to be studied and analysed after the cycling process. Their stability, or not, will determine the suitability of the alloy for being used as latent heat TES material.

## Methodology

### Material synthesis

Table 1 provides the composition of the selected five PCMs, which are eutectic mixtures of Mg, Zn and Al metals. For ease of reading the Zn<sub>84</sub>Al<sub>8.7</sub>Mg<sub>7.3</sub>, Zn<sub>88.7</sub>Al<sub>11.3</sub>, Zn<sub>92.2</sub>Mg<sub>7.8</sub>, Mg<sub>72</sub>Zn<sub>28</sub> and Mg<sub>70</sub>Zn<sub>24.9</sub>Al<sub>5.1</sub>, metal alloys have been called A, B, C, D and E, respectively. Ingots of Mg and Zn, supplied by Alealsa S.A., and pellets of 3–12 mm of Al, delivered by Sigma-Aldrich, with purity level higher than 99.99% were used. Around 60 g of alloy samples were prepared by stoichiometric proportions of small pieces of the primary metals according to each alloy theoretical composition. The compounds were placed into

**Table 1** Theoretical melting temperature and composition, in atomic and mass percentages, of the selected PCM candidates

Candidate	Theoretical melting temperature/°C	Eutectic composition/at.%	mass%
A	345	Zn <sub>84</sub> Al <sub>8.7</sub> Mg <sub>7.3</sub>	93.9Zn–3.7Al–2.4Mg
B	380	Zn <sub>88.7</sub> Al <sub>11.3</sub>	95Zn–5Al
C	370	Zn <sub>92.2</sub> Mg <sub>7.8</sub>	97Zn–3Mg
D	340	Mg <sub>72</sub> Zn <sub>28</sub>	49Mg–51Zn
E	338	Mg <sub>70</sub> Zn <sub>24.9</sub> Al <sub>5.1</sub>	49Mg–47Zn–4Al

open alumina crucibles located inside small stainless steel reactors, which were later closed hermetically in a glove box under argon inert atmosphere to avoid any possible oxidation. The melting process was performed in a muffle furnace during 6 h at 450 °C for Mg<sub>72</sub>Zn<sub>28</sub> and Mg<sub>70</sub>Zn<sub>24.9</sub>Al<sub>5.1</sub> alloys and at 500 °C for Zn<sub>84</sub>Al<sub>8.7</sub>Mg<sub>7.3</sub>, Zn<sub>88.7</sub>Al<sub>11.3</sub>, Zn<sub>92.2</sub>Mg<sub>7.8</sub> compositions. To increase the homogeneity of the sample, every 30 min the steel reactors were briefly taken out from the furnace and stirred by circular movements in the horizontal axis. After the cooling process, the samples were turned upside down and were melted again. This last process was repeated three times to ensure the homogeneity of the samples. The last cooling process to room temperature was carried out at cooling rate of 10 °C min<sup>-1</sup>.

#### Accelerated thermal stability test

To analyse the thermal stability of the studied PCMs, an accelerated cycling behaviour has been studied, by using an increased heating/cooling rate compared to the rate used in real applications. For this purpose, two kinds of cycling methodologies have been followed. On the first stage, a short-term test was carried out by using differential scanning calorimeter (DSC) up to 100 cycles. On the second stage, a long-term test by using a high-temperature electrical furnace was performed up to 500 cycles.

#### *Short-term thermal stability: thermal cycling test using a differential scanning calorimeter (DSC)*

The five PCM candidates were subjected to consecutive melting/solidification cycles by using a differential scanning calorimeter (DSC) (TA Q2000 calorimeter). For this purpose, small pieces of around 100 mg were cut by diamond saw from the synthesized samples. Then, the samples were subjected to 100 melting/solidification thermal cycles from 300 to 450 °C inside open alumina crucibles, with heating/cooling rates of 10 °C min<sup>-1</sup> and under protective argon flow (100 mL min<sup>-1</sup>). The phase change temperature and the latent heat of each cycle were continuously

recorded with an experimental error of ±0.01 °C and ±0.1%, respectively.

#### *Long-term thermal stability: thermal cycling test by electrical furnace*

The thermal cycling tests of binary and ternary eutectic alloys, in particular, D and E compositions, were also performed by a tubular muffle electrical furnace. The synthesized samples of around 100 g were put in alumina open crucibles, and then, the systems (crucible and sample) were introduced inside of a quartz tube in order to conduct the experiments under a protective argon flux (100 mL min<sup>-1</sup>) to avoid any oxidation process. In each melting/solidification cycle, heating/cooling rate of 10 °C min<sup>-1</sup> was applied between 300 and 450 °C, with isothermal steps of 10 min at minimum and maximum temperatures (300 and 450 °C). The samples of both materials were subjected to a total of 500 melting/solidification cycles. During the experiments, the cycling was interrupted after 50, 100, 300 and 500 thermal cycles, and small pieces of around 5 g were cut from the bulk by a diamond saw in order to analyse any changes in the thermophysical properties and the microstructure of the materials.

In this way, the phase change temperature and latent heat were determined by DSC analysis. For this purpose, pieces of around 100 mg of the samples were cycled 3 times in open alumina crucibles between 200 and 450 °C, with heating/cooling rates of 10 °C min<sup>-1</sup> and under protective argon flow of 100 mL min<sup>-1</sup>.

#### Scanning electron microscopy analysis

The microstructure investigation of the samples subjected to long-term tests was performed by scanning electron microscopy (SEM), using a Quanta FEG 250 microscope operated at high vacuum mode at 30 kV and with a back-scattered electron detector (BSED). For these analyses, smooth surfaces of untreated samples and samples after 50, 100, 300 and 500 thermal cycles were prepared by using

diamond paste down to 3  $\mu\text{m}$  grain size and then cleaned by an acetone ultrasonic bath at room temperature during 10 min.

## Results and discussion

### Short-term thermal stability tests

The five candidate samples have been cycled for 100 times, and their phase change temperatures and heat of fusion have been continuously recorded. The phase change temperatures, heat of fusion and their relative percentage difference (RPD), with respect to first reference cycle of  $\text{Zn}_{84}\text{Al}_{8.7}\text{Mg}_{7.3}$  (A),  $\text{Zn}_{88.7}\text{Al}_{11.3}$  (B),  $\text{Zn}_{92.2}\text{Mg}_{7.8}$  (C),  $\text{Zn}_{72}\text{Mg}_{28}$  (D) and  $\text{Mg}_{70}\text{Zn}_{24.9}\text{Al}_{5.1}$  (E), are shown in Tables 2–6, respectively. For the sake of simplicity, only one set after each 10 successive cycles was presented. The RPD between each property  $i$  of the material at any number of cycle  $n$  and the first cycle can be defined as:

$$\text{RPD} = \frac{x_{n,i} - x_{1,i}}{x_{1,i}} \times 100(\%) \quad (1)$$

where  $x_{n,i}$  is the value of the given property after  $n$  cycles, and  $x_{1,i}$  is the value of this property at first cycle.

The first column of the tables shows the number of the cycle. The second and third columns show the melting onset temperature and its RPD (%) with respect to the first cycle. The fourth and fifth columns present the melting peak temperature with its RPD (%) value. The sixth column indicates the melting range temperature used as limits to calculate the heat of fusion. It has to be noted that this range from DSC comes from the dynamic nature of the experiment. Due to the eutectic nature of the alloys, the

melting process takes place at isothermal temperature, but the range is expected in dynamic measurements. The seventh and eighth columns show the calculated heat of fusion and its RPD (%) value. Finally, the last column presents the thermal hysteresis observed in the solidification process.

The results obtained after analysis of sample A are presented in Table 2, from which it can be seen that the first cycle has a melting onset temperature of 343.69  $^{\circ}\text{C}$ , and no remarkable variations were observed after 100 cycles of testing. Thereby, the maximum RPD value calculated was 0.16% for the tenth cycle, which it can be evaluated as negligible in the frame of a possible application of this alloy as latent heat storage material. Regarding the peak temperature, no relevant variations can be observed up to 90th cycle, where the peak temperature is reduced in a 0.6%.

The average melting temperature range has been taken from 336.40 to 384.61  $^{\circ}\text{C}$ . On the other hand, the heat of fusion for sample A was calculated for the melting temperature ranges obtained in each cycle, being 131.5  $\text{J g}^{-1}$  as it is indicated in the first cycle. Regarding the RPD, its value gradually decreases with the thermal cycling from 0.15% in the 20th cycle to 1.90% in the 100th cycle. So, the heat of fusion of the eutectic phase transition in sample A decreases 2.5  $\text{J g}^{-1}$  after 100 cycles. Finally, the thermal hysteresis values are almost constant and present an average value of 12.45  $^{\circ}\text{C}$ .

Sample B presented similar results to sample A after thermal cycling, as may be observed in Table 3. The melting onset temperature and peak temperature were measured before cycling, obtaining values of 381.71 and 394.64  $^{\circ}\text{C}$ , respectively. After 100 cycles, the calculated RPD values were under 0.01% for onset temperature and under 0.76% for peak temperature, which can be

**Table 2** Latent heat of fusion, melting onset temperature and undercooling degrees of candidate A ( $\text{Zn}_{84}\text{Al}_{8.7}\text{Mg}_{7.3}$ ) at different numbers of thermal cycles measured by DSC

No. of cycles	Onset temperature/ $^{\circ}\text{C}$		Peak temperature/ $^{\circ}\text{C}$		Melting range/ $^{\circ}\text{C}$	Heat of fusion/ $\text{J g}^{-1}$		Undercooling/ $^{\circ}\text{C}$
		RPD/%		RPD/%			RPD/%	
1	343.69	–	354.72	–	336.91–379.88	131.5	–	11.39
10	344.25	0.16	354.93	0.06	335.79–387.45	131.5	0	12.97
20	343.84	0.04	355.04	0.09	338.69–380.10	131.3	–0.15	12.41
30	343.87	0.05	354.98	0.07	336.68–390.34	131.6	0.08	12.57
40	343.82	0.04	354.74	0.01	337.80–383.22	131.2	–0.23	12.38
50	343.86	0.05	354.78	0.02	334.01–384.78	130.8	–0.53	12.57
60	343.85	0.05	354.76	0.01	335.13–382.55	130.8	–0.53	12.41
70	343.89	0.06	354.78	0.02	336.02–387.23	130.2	–0.99	12.54
80	343.91	0.06	354.79	0.02	336.24–385.67	129.5	–1.52	12.60
90	343.89	0.06	352.66	–0.58	334.22–386.72	129.3	–1.67	12.66
100	343.88	0.06	352.62	–0.59	338.91–382.77	129.0	–1.90	12.41

**Table 3** Latent heat of fusion, melting onset temperature and undercooling degrees of candidate B ( $Zn_{88.7}Al_{11.3}$ ) at different numbers of thermal cycles measured by DSC

No. of cycles	Onset temperature/ $^{\circ}C$		Peak temperature/ $^{\circ}C$		Melting range/ $^{\circ}C$	Heat of fusion/ $J g^{-1}$		Undercooling/ $^{\circ}C$
		RPD/%		RPD/%			RPD/%	
1	381.72	–	394.64	–	374.49–420.89	118.4	–	4.75
10	381.69	–0.01	394.89	–0.69	376.88–415.17	119.2	0.68	4.68
20	381.70	–0.01	394.84	–0.70	376.28–416.05	119.1	0.59	4.75
30	381.71	0.00	394.74	–0.73	377.01–416.05	119.5	0.93	5.24
40	381.71	0.00	394.71	–0.74	377.01–417.79	119.5	0.93	4.96
50	381.71	0.00	394.70	–0.74	376.76–417.66	119.7	1.10	4.93
60	381.73	0.003	394.68	–0.74	376.51–420.77	119.9	1.27	4.85
70	381.72	0.00	394.64	–0.75	376.39–415.42	119.7	1.10	4.91
80	381.70	–0.01	394.63	–0.76	377.26–414.80	119.7	1.10	4.89
90	381.73	0.00	394.62	–0.76	377.63–415.05	119.7	1.10	5.84
100	381.72	0.00	394.60	–0.76	376.14–415.30	119.9	1.27	6.52

considered an almost negligible variation when the material is evaluated as PCM candidate in a TES application.

The average melting range to calculate the heat of fusion is  $376.07$ – $416.12$   $^{\circ}C$ . In this case, the heat of fusion for the first cycle is  $118.4$   $J g^{-1}$  and it increases up to  $119.9$   $J g^{-1}$  after 100 cycles. Finally, the thermal hysteresis, which is apparently very small, experiences almost negligible variations during the thermal cycling, being in a range between  $4.68$  and  $6.52$   $^{\circ}C$ , taking an average value of  $5.12$   $^{\circ}C$ .

Thermal cycling results of the sample C are shown in Table 4. The melting onset temperature of  $370.36$   $^{\circ}C$  and the peak temperature of  $382.52$   $^{\circ}C$  are obtained and maintained constant during the thermal cycling, where the maximum RPD values are  $0.21$  and  $0.80\%$ , respectively. For the average melting range of  $362.88$ – $411.40$   $^{\circ}C$ , with

RPD values  $<0.73$  and  $0.63\%$ , respectively, the heat of fusion of sample C decreases after 100 thermal cycles from  $106.4$  to  $85.39$   $J g^{-1}$ . The heat of fusion shows a progressive decrease with the thermal cycling and a RPD value of around  $19.75\%$  after 100 thermal cycles. On the other hand, the subcooling increases from  $4.53$   $^{\circ}C$  in the first cycle up to  $9.53$   $^{\circ}C$  in the tenth. Afterwards, its value remains constant, with an average value of  $9.30$   $^{\circ}C$ .

The results of sample D are shown in Table 5, and this material presents similar behaviour to sample A. The melting onset temperature of  $341.07$   $^{\circ}C$  and the peak temperature of  $349.57$   $^{\circ}C$  are constant during the thermal cycling, where the RPD values are  $<0.28$  and  $1.15\%$ , respectively. The heat of fusion has been calculated in the average melting range of  $337.63$ – $381.19$   $^{\circ}C$ . Its value

**Table 4** Latent heat of fusion, melting onset temperature and undercooling degrees of candidate C ( $Zn_{92.2}Mg_{7.8}$ ) at different numbers of thermal cycles measured by DSC

No. of cycles	Onset temperature/ $^{\circ}C$		Peak temperature/ $^{\circ}C$		Melting range/ $^{\circ}C$	Heat of fusion/ $J g^{-1}$		Undercooling/ $^{\circ}C$
		RPD/%		RPD/%			RPD/%	
1	370.36	–	382.52	–	362.94–418.44	106.4	–	4.53
10	370.74	0.10	382.51	0.00	362.73–409.67	105.3	–1.03	9.17
20	370.50	0.04	382.50	–0.01	365.73–408.92	102.3	–3.85	9.07
30	370.94	0.16	381.13	–0.36	364.21–409.05	101.7	–4.42	9.53
40	370.54	0.05	379.47	–0.80	362.65–410.16	98.51	–7.42	9.17
50	370.59	0.06	379.59	–0.77	362.65–411.27	96.39	–9.41	9.19
60	370.65	0.08	381.10	–0.37	365.09–410.16	93.99	–11.66	9.15
70	371.14	0.21	381.14	–0.36	362.21–411.27	91.59	–13.92	9.71
80	371.05	0.19	381.32	–0.31	360.65–409.49	89.61	–15.78	9.58
90	370.52	0.04	381.43	–0.28	362.65–411.03	87.03	–18.20	9.07
100	370.48	0.03	380.01	–0.66	362.87–411.71	85.39	–19.75	8.98

**Table 5** Latent heat of fusion, melting onset temperature and undercooling degrees of candidate D ( $\text{Mg}_{72}\text{Zn}_{28}$ ) at different numbers of thermal cycles measured by DSC

No. of cycles	Onset temperature/ $^{\circ}\text{C}$		Peak temperature/ $^{\circ}\text{C}$		Melting range/ $^{\circ}\text{C}$	Heat of fusion/ $\text{J g}^{-1}$		Undercooling/ $^{\circ}\text{C}$
		RPD/%		RPD/%			RPD/%	
1	341.07	–	349.57	–	337.48–380.11	152.7	–	7.17
10	341.84	0.23	351.34	0.51	336.95–384.80	152.8	0.07	7.75
20	341.93	0.25	352.98	0.98	338.65–382.98	152.5	–0.13	7.64
30	341.97	0.26	353.14	1.02	337.08–381.49	151.8	–0.59	9.01
40	342.00	0.27	353.31	1.07	337.70–382.88	151.5	–0.79	9.04
50	341.98	0.27	353.37	1.09	336.84–383.62	151.5	–0.79	9.04
60	341.98	0.27	353.59	1.15	337.91–381.60	151.3	–0.92	9.05
70	342.03	0.28	353.44	1.11	338.12–380.32	151.2	–0.98	9.17
80	342.00	0.27	353.42	1.10	337.38–378.83	150.8	–1.24	9.15
90	341.24	0.05	353.32	1.07	337.70–379.25	150.5	–1.44	8.42
100	341.22	0.04	353.28	1.06	338.12–377.55	150.1	–1.70	8.38

decreases slightly from 152.7 to 150.1  $\text{J g}^{-1}$ , representing a progressive decrease of around 1.70% after 100 thermal cycles. On the other hand, the thermal hysteresis increases from 7.17  $^{\circ}\text{C}$  in the first cycle up to 9.01  $^{\circ}\text{C}$  in the 30th cycle and then its value remains approximately constant after 100 cycles, with an average value of 8.53  $^{\circ}\text{C}$ .

Finally, the results of sample E are presented in Table 6, showing a constant melting onset temperature and peak temperatures of around 339.98 and 348.30  $^{\circ}\text{C}$ , with RPD values <0.11 and 0.40%, respectively. As in results of samples A and D, it can be observed a slight and progressive decrease in the heat of fusion with cycling. Regarding the enthalpy, sample E shows a slight decrease from 159.6 to 158.9  $\text{J g}^{-1}$ , corresponding to a reduction of 0.44% after 100 thermal cycles, which can be considered

negligible. The thermal hysteresis degrees are approximately constant with an average value of 9.05  $^{\circ}\text{C}$ .

Figures 1 and 2 display the melting and solidification curves, obtained by DSC, corresponding to the 1st, 25th, 50th 75th and 100th cycles of samples B and C. As it may be observed, the form of first cycle curve in each sample differs from the rest of the cycles, which can be attributed to the change of the contact surface between the sample and the bottom of the alumina crucible. However, the sample B shows consistent repeatability, whereas in the case of sample C, it can be clearly observed a progressive formation of a secondary peak before the main peak, indicated by arrow in the solidification curves, for the 50th, 75th and 100th cycles, which corresponds to a solidification of another phase. However, this fact may be explained

**Table 6** Latent heat of fusion, melting onset temperature and undercooling degrees of candidate E ( $\text{Mg}_{70}\text{Zn}_{24.9}\text{Al}_{5.1}$ ) at different numbers of thermal cycles measured by DSC

No. of cycles	Onset temperature/ $^{\circ}\text{C}$		Peak temperature/ $^{\circ}\text{C}$		Melting range/ $^{\circ}\text{C}$	Heat of fusion/ $\text{J g}^{-1}$		Undercooling/ $^{\circ}\text{C}$
		RPD/%		RPD/%			RPD/%	
1	339.98	–	348.30	–	337.48–379.66	159.6	–	8.79
10	340.00	0.01	348.98	0.20	336.31–379.87	159.5	–0.06	8.61
20	340.34	0.11	348.38	0.02	337.27–379.56	159.4	–0.13	8.19
30	340.32	0.10	349.00	0.20	336.18–379.88	159.0	–0.38	9.11
40	340.13	0.04	348.51	0.06	336.95–379.57	159.2	–0.25	8.71
50	340.31	0.10	349.03	0.21	336.10–379.34	158.8	–0.50	9.65
60	340.10	0.04	349.09	0.23	335.78–379.45	158.8	–0.50	9.38
70	340.21	0.07	349.06	0.22	337.27–380.30	158.9	–0.44	8.81
80	340.20	0.06	349.12	0.24	337.59–380.30	158.8	–0.50	9.28
90	340.26	0.08	349.08	0.22	336.42–380.73	158.8	–0.50	9.44
100	340.37	0.11	349.69	0.40	337.16–380.41	158.9	–0.44	9.54



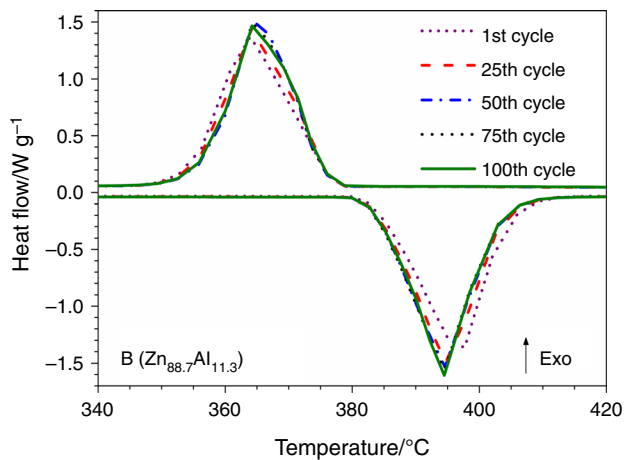


**Fig. 1** Melting and solidification DSC curves after 1, 25, 75 and 100 thermal cycles of the candidate B ( $\text{Zn}_{88.7}\text{Al}_{11.3}$ )

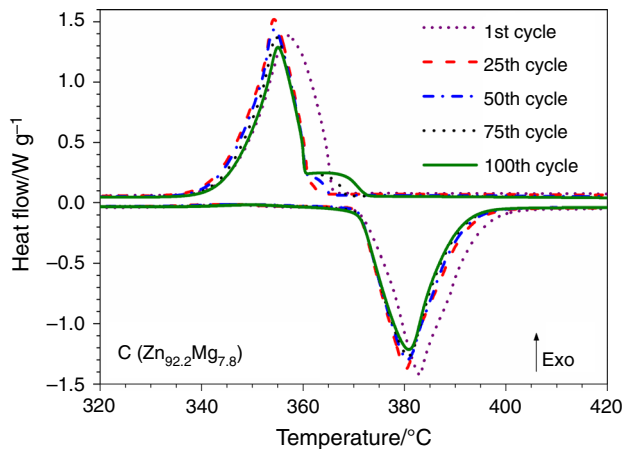


**Fig. 2** Melting and solidification DSC curves after 1, 25, 75 and 100 thermal cycles of candidate C ( $\text{Zn}_{92.2}\text{Mg}_{7.8}$ )

by the competitive growth between a  $\text{Zn-MgZn}_2$  metastable phase and  $\text{Zn-Mg}_2\text{Zn}_{11}$  stable phase observed for  $\text{Zn}_{92.2}\text{Mg}_{7.8}$  by Akdepniz et al. [32]. Nevertheless, further investigations are ongoing in our laboratory to confirm this hypothesis. In any case, the formation of this secondary peak indicates that the phase transition of the C sample is not totally congruent.

In summary, all the studied materials show some changes in melting and solidification temperatures accompanied with some changes of the heat of fusion. In this way, A, B, D and E candidates show negligible changes in their heat of fusion of 1.90, 1.27, 1.70 and 0.44%, respectively. In the case of sample C, the substantial fusion heat reduction of 19.75% is due to non-congruent phase transition as it can be seen by the progressive secondary peak formation before the eutectic solidification peak in Fig. 2. Furthermore, it can be concluded that A, B, D and E alloys show a congruent phase transition despite the slight enthalpy reduction, which can

be attributed to slight oxidations produced during the experiments.

### Long-term thermal stability tests

The melting/solidification DSC curves of samples D and E after 1, 50, 100, 300 and 500 thermal cycles are shown in Figs. 3 and 4. By simple comparison of the curves of each sample, a good thermal stability of the materials can be observed. The melting peaks of sample D in Fig. 3 show a secondary peak before the eutectic melting process. This peak corresponds to a solid  $\rightarrow$  solid phase transition ( $\text{Mg}_7\text{Zn}_3 + \text{Mg} \rightarrow \text{Mg}_{21}\text{Zn}_{25}$ ). This phase transition is predicted by Mg–Zn phase diagram and has been experimentally confirmed in [1]. Due to the overlapping of the secondary and the melting peaks, the heat of fusion listed in Table 7 has been calculated from both transformations.

Table 7 shows the long-term thermal stability results of sample D. No changes are observed in the melting onset temperature of  $340.38^\circ\text{C}$  and peak temperature of  $347.22^\circ\text{C}$  after the 500 thermal cycles, where their RPD values are  $<0.21$  and  $1.79\%$ , respectively. The thermal hysteresis changes between  $7.82$  and  $9.59^\circ\text{C}$ , with an average value of  $8.55^\circ\text{C}$ . The value of the heat of fusion oscillates during the thermal cycling around the value of untreated sample, i.e. no

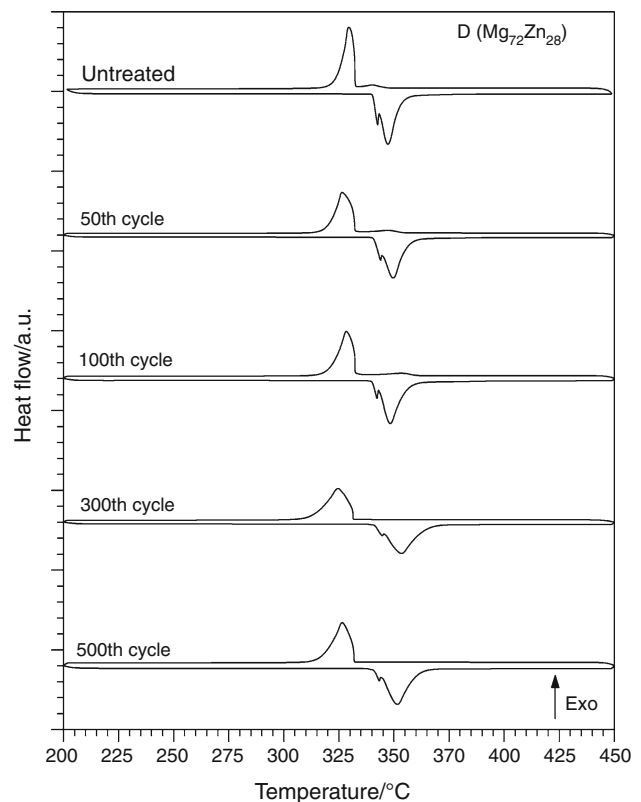


**Fig. 3** Melting and solidification DSC curves of candidate D ( $\text{Mg}_{72}\text{Zn}_{28}$ ) for after 0, 50, 100, 300 and 500 thermal cycles

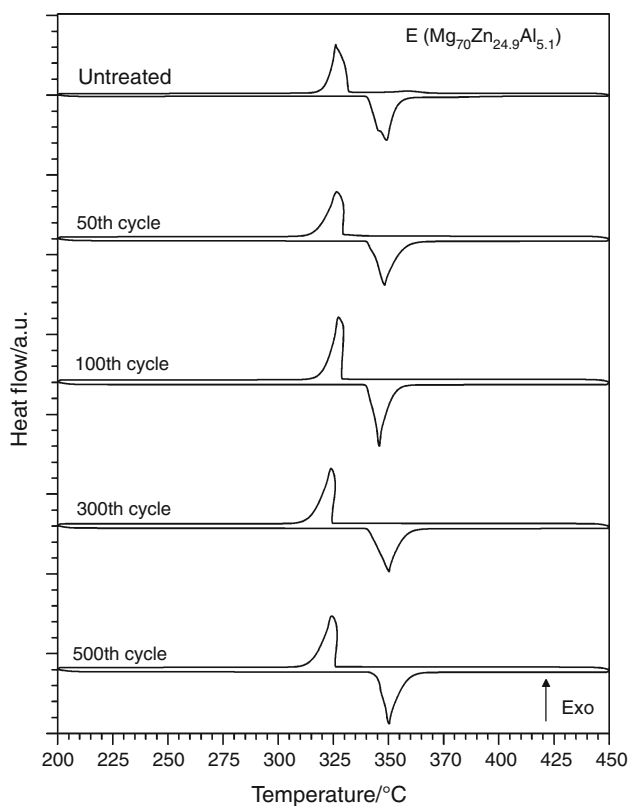


**Fig. 4** Melting and solidification DSC curves of candidate E ( $\text{Mg}_{70}\text{Zn}_{24.9}\text{Al}_{5.1}$ ) after 0, 50, 100, 300 and 500 thermal cycles

cycled sample ( $154.9 \text{ J g}^{-1}$ ). However, no decreasing trend with the increase in the number of cycles is observed. Thereby, this oscillation may be due to the experimental error coming from the use of different pieces of the sample. On the other hand, the observed RPD value of 0.39% after 500 cycles can be considered negligible. Thus, it can be considered that alloy D presents a congruent phase transition after 500 thermal cycles, maintaining practically constant its phase change temperature and heat of fusion.

Finally, Table 8 shows the long-term thermal stability results of candidate E. In the untreated sample, the melting onset temperature is  $341.09 \text{ }^\circ\text{C}$ . This temperature is reproducible during the thermal cycling, where the RPD values for onset and peak temperatures do not exceeded 0.53 and 1.10%, respectively. In this case, thermal hysteresis temperatures show higher differences than in short-term thermal cycling and fluctuate between  $6.73$  and  $16.01 \text{ }^\circ\text{C}$  without detecting any continuous increasing trend on the values with the increase in the cycle number. The average melting range used for the heat of fusion calculation is between  $336.64$  and  $383.06 \text{ }^\circ\text{C}$ . After the first cycle, the heat of fusion increases its value from  $152.9 \text{ J g}^{-1}$  (first cycle) to  $155.2 \text{ J g}^{-1}$  (50th cycle), and then, it remains practically constant up to 500 cycles. So, it can be concluded that the alloy E also presents a congruent phase transition after 500 cycles.

In order to analyse the microstructure evolution of the candidate E, SEM analysis has been carried out for the

**Table 7** Latent heat of fusion, melting onset temperature and undercooling degrees of candidate D ( $\text{Mg}_{72}\text{Zn}_{28}$ ) cycled in electrical furnace

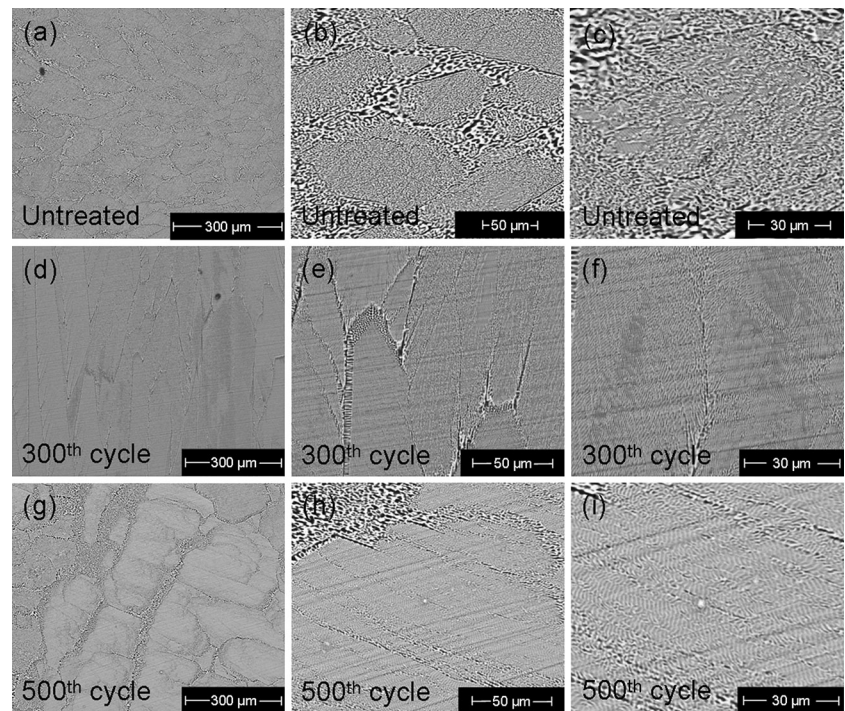
No. of cycles	Onset temperature/ $^\circ\text{C}$		Peak temperature/ $^\circ\text{C}$		Melting range/ $^\circ\text{C}$	Heat of fusion/ $\text{J g}^{-1}$		Undercooling/ $^\circ\text{C}$
	RPD/%	RPD/%	RPD/%	RPD/%				
1	340.38	–	347.22	–	337.38–381.70	154.9	–	7.98
50	340.84	0.14	349.59	0.68	336.99–386.47	153.3	–1.03	8.60
100	340.15	–0.07	348.32	0.32	337.61–386.48	155.4	0.32	7.82
300	341.09	0.21	353.43	1.79	336.50–380.38	153.6	–0.84	9.59
500	340.64	0.08	351.54	1.24	336.99–374.41	154.3	–0.39	8.78

**Table 8** Latent heat of fusion, melting onset temperature and undercooling degrees of candidate E ( $\text{Mg}_{70}\text{Zn}_{24.9}\text{Al}_{5.1}$ ) cycled in electrical furnace

No. of cycles	Onset temperature/ $^\circ\text{C}$		Peak temperature/ $^\circ\text{C}$		Melting range/ $^\circ\text{C}$	Heat of fusion/ $\text{J g}^{-1}$		Undercooling/ $^\circ\text{C}$
	RPD/%	RPD/%	RPD/%	RPD/%				
1	341.09	–	349.38	–	336.88–386.50	152.9	–	8.18
50	340.28	–0.24	348.12	–0.36	337.74–382.35	155.2	0.84	11.97
100	339.29	–0.53	345.55	–1.10	336.85–387.96	156.8	1.88	10.80
300	340.80	–0.09	350.21	0.24	336.30–380.97	154.9	0.65	16.01
500	340.62	–0.14	348.60	–0.22	335.41–377.52	156.1	1.43	6.73



**Fig. 5** SEM images of candidate E ( $\text{Mg}_{70}\text{Zn}_{24.9}\text{Al}_{5.1}$ ), untreated and after 300 and 500 thermal cycles at  $\times 300$  ( $300\ \mu\text{m}$ ),  $\times 1500$  ( $50\ \mu\text{m}$ ) and  $\times 3000$  ( $30\ \mu\text{m}$ ) magnifications



untreated sample and after 50, 100, 300 and 500 cycles. Figure 5 shows at different magnifications the microstructure of untreated sample and after 300 and 500 cycles. The microstructure of untreated sample is displayed in Fig. 5a–c. The eutectic microstructure with  $\text{Mg}_{21}\text{Zn}_{25}$  intermetallic phase in light grey colour and the Mg solid solution in dark grey colour can be observed. The eutectic microstructure of samples after 300 and 500 cycles is displayed in Fig. 5d–i, where the stability of their microstructures can be clearly observed. Thus, from these results it can be concluded that no chemical degradation or segregation in candidate E after 500 cycles has been detected.

## Conclusions

The thermal stability of five eutectic metal alloys as potential high-temperature PCMs has been evaluated in this work. Short-term thermal cycling tests of 100 cycles have been carried out for all the candidates, and long-term cycling tests of 500 cycles for candidates D and E have been performed. The changes on melting temperatures, heat of fusion and thermal hysteresis have been analysed using the DSC technique in all cases. The changes in eutectic microstructure have been analysed by SEM for candidate E.

Thereby, after short-term cycling tests of 100 cycles, no variations on the onset melting and solidification temperatures of the five materials have been obtained. The heat of

fusion shows negligible changes, which in some cases may be due to the small oxidation of the samples. An enthalpy reduction accompanied with a progressive formation of a secondary peak before solidification peak is observed for sample C. Thus, in this case, the phase transition is not totally congruent, probably caused by the solidification of metastable phase.

After long-term thermal cycling tests of 500 cycles, alloy D ( $\text{Mg}_{72}\text{Zn}_{28}$ ) does not show changes in its melting temperature of  $340.38\ ^\circ\text{C}$ . The heat of fusion value of  $154.9\ \text{J g}^{-1}$  oscillated during the thermal cycles; however, no decreasing trend with the increase in the cycle number is observed, where the RPD of 0.39% after 500 cycles can be considered negligible. In the same way, candidate E ( $\text{Mg}_{70}\text{Zn}_{24.9}\text{Al}_{5.1}$ ) presents no changes in its melting temperature of  $341.09\ ^\circ\text{C}$ . The heat of fusion value of  $152.9\ \text{J g}^{-1}$  increases from first to tenth cycle and then fluctuates, showing an increase of 1.43% after 500 cycles. Besides, the SEM analysis performed in sample E after 300 and 500 cycles shows stable eutectic microstructure without any chemical degradation or segregation of the phases. Thus, based on these results, the phase transition can be considered congruent for samples D and E after long-term thermal cycling tests of 500 cycles.

Based on the performed thermal cycling test in this work, it can be concluded that the A ( $\text{Zn}_{84}\text{Al}_{8.7}\text{Mg}_{7.3}$ ), B ( $\text{Zn}_{88.7}\text{Al}_{11.3}$ ), D ( $\text{Mg}_{72}\text{Zn}_{28}$ ) and E ( $\text{Mg}_{70}\text{Zn}_{24.9}\text{Al}_{5.1}$ ) eutectic alloys are thermally stable and can be used as promising PCMs for TES systems.

**Acknowledgements** The authors would like to thank the Department of Industry, Innovation, Commerce and Tourism of the Basque Government for funding the ETORTEK CIC Energigune-2011 and ETORTEK CIC Energigune-2014 research programs. The authors would also like to thank Naira Soguero and Jon Ajuria for their technical support.

## References

- Rodríguez-Aseguinolaza J, Blanco-Rodríguez P, Risueño E, Tello MJ, Doppiu S. Thermodynamic study of the eutectic Mg49–Zn51 alloy used for thermal energy storage. *J Therm Anal Calorim.* 2014;117:93–9.
- Sharma A, Tyagi VV, Chen CR, Buddhi D. Review on thermal energy storage with phase change materials and applications. *Renew Sustain Energy Rev.* 2009;13:318–45.
- Farid MM, Khudhair AM, Razack SAK, Al-Hallaj S. A review on phase change energy storage: materials and applications. *Energy Convers Manag.* 2004;45:1597–615.
- Michels H, Pitz-Paal R. Cascade latent heat storage for parabolic trough solar power plants. *Sol Energy.* 2007;81:829–37.
- Seeniraj RV, Narasimhan NL. Performance enhancement of a solar dynamic LHTS module having both fins and multiple PCMs. *Sol Energy.* 2008;82:535–42.
- Nomura T, Okinaka N, Akiyama T. Waste heat transportation system, using phase change materials (PCM) from steelworks to chemical plant. *Resour Conserv Recycl.* 2010;54:1000–6.
- Kenisarin MM. High-temperature phase change materials for thermal energy storage. *Renew Sustain Energy Rev.* 2010;14:955–70.
- Liu M, Saman W, Bruno F. Review on storage materials and thermal performance enhancement techniques for high temperature change thermal storage systems. *Renew Sustain Energy Rev.* 2012;16:2118–32.
- Laing D, Bahl C, Bauer T, Lehmann D, Steinmann W-D. Thermal energy storage for direct steam generation. *Sol Energy.* 2011;85:627–33.
- Liu M, Belusko M, Steven Tay NH, Bruno F. Impact of the heat transfer fluid in a flat plate phase change thermal Storage unit for concentrated solar tower plants. *Sol Energy.* 2014;101:220–31.
- Cardenas B, León N. High temperature latent heat thermal energy storage: phase change materials, desing considerations and performance enhancement techniques. *Renew Sustain Energy Rev.* 2013;27:724–37.
- Khare S, Dell'Amico M, Knight C, McGarry S. Selection of materials from high temperature latent heat energy storage. *Sol Energy Mater Sol C.* 2012;107:20–7.
- Hoshi A, Mills DR, Bittar A, Saitoh TS. Screening of high melting point phase change materials (PCM) in solar thermal concentrating technology based on CLFR. *Sol Energy.* 2005;79:332–9.
- Rathod MK, Banerjee J. Thermal stability phase change materials used in latent heat energy storage systems: a review. *Renew Sustain Energy Rev.* 2013;18:246–58.
- Sari A, Karaipekli A. Preparation, thermal properties and thermal reliability of palmitic acid/expanded graphite composite as form-stable PCM for thermal energy storage. *Sol Energy Mater Sol C.* 2009;93:571–6.
- Sari A. Eutectic mixture of some fatty acids for latent heat storage: thermal properties and thermal reliability with respect to thermal cycling. *Energy Convers Manag.* 2006;47:1207–21.
- Sari A, Sari H, Önal A. Thermal properties and thermal reliability of eutectic mixtures of some fatty acids as latent heat storage materials. *Energy Convers Manag.* 2004;45:365–76.
- El-Sebaai AA, Al-Amir S, Al-Marzouki FM, Faidah AS, Al-Ghamdi AA, Al-Heniti S. One thousand thermal cycles magnesium chloride hexahydrate as a promising PCM for indoor solar cooking. *Energy Convers Manag.* 2011;52:1771–7.
- Tyagi VV, Buddhi D. Thermal cycle testing of calcium chloride hexahydrate as a possible PCM for latent heat storage. *Sol Energy Mater Sol C.* 2008;92:891–9.
- Sharma A, Sharma SD, Buddhi D. Accelerated thermal cycle test of acetamide, stearic acid and paraffin wax for solar thermal latent heat storage applications. *Energy Convers Manag.* 2002;43:1923–30.
- Sari A. Thermal reliability test of some fatty acids as PCMs used for solar thermal latent heat storage applications. *Energy Convers Manag.* 2003;44:2277–87.
- Shukla A, Buddhi D, Sawhney RL. Thermal cycling test of few selected inorganic and organic phase change materials. *Renew Energy.* 2008;33:2606–14.
- Sharma SD, Buddhi D, Sawhney RL. Accelerated thermal cycle test of latent heat-storage materials. *Sol Energy.* 1999;66:483–90.
- Genc ZK, Canbay CA, Acar SS, Sekerci M, Genc M. Preparation and thermal properties of heterogeneous composite phase change materials based on camphene–palmitic acid. *J Therm Anal Calorim.* 2015;120(3):1679–88.
- Sharma RK, Ganesan P, Tyagi VV. Long-term thermal and chemical reliability study of different organic phase change materials for thermal energy storage applications. *J Therm Anal Calorim.* 2016;124(3):1357–66.
- Fu X, Liu Z, Wu B, Wang J, Lei J. Preparation and thermal properties of stearic acid/diatomite composites as form-stable phase change materials for thermal energy storage via direct impregnation method. *J Therm Anal Calorim.* 2016;123(2):1173–81.
- Shin BC, Kim SD. Ternary carbonate eutectic (lithium, sodium and potassium carbonates) for latent heat storage medium. *Sol Energy Mater.* 1990;21:81–90.
- Sun JQ, Zhang RY, Liu ZP, Lu GH. Thermal reliability test of Al–34%Mg–6%Zn alloy as latent heat storage material and corrosion of metal with respect to thermal cycling. *Energy Convers Manag.* 2007;48(2):619–24.
- Kuravi S, Trahan Yogi Goswami JD, Rahman MM, Stefanakos EK. Thermal energy storage technologies and systems for concentrating solar power plants. *Prog Energy Combust Sci.* 2013;39:285–319.
- Alam TE, Dhau JS, Yogi Goswami D, Stefanakos E. Macroencapsulation and characterization of phase change materials for latent heat thermal energy storage systems. *Appl Energy.* 2015;154:92–101.
- Liu M, Gomez JC, Turchi CS, Tay NHS, Saman W, Bruno F. Determination of thermo-physical properties and stability testing of high-temperature phase-change materials as CSP applications. *Sol Energy Mater Sol C.* 2015;139:81–7.
- Akdepniz MV, Wood JV. Microstructures and phase selection in rapidly solidified Zn–Mg alloys. *J Mater Sci.* 1996;31:545–50.